Chapter 1

Parametric Study

1.1 Introduction

In this chapter CFD is used to examine the performance of di¤erent downwind sail designs in two dimensions. In this study a series of di¤erent sail designs are analysed and by varying draft and camber. The design study is performed on a solitary downwind sail, which ignores the in‡uence of the mainsail. The base sail shape is also tested with a mainsail included in order to establish the impact of the mainsail presence and to determine whether downwind sails can be designed (in two-dimensions) without considering the presence of the mainsail.

1.1.1 Sail sections

A sail section with it's de…ning geometry is illustrated in Figure 1.1. The sail shapes used in this study are described by the following parameters: draft, camber, front percentage, back percentage, leading edge slope and trailing edge slope. These parameters are de…ned as follows:

Camber = $\frac{y_{max}}{c}$; where y_{max} is the greatest distance of the sail o¤ the chord line.

Draft = $\frac{x_d}{c}$; where x_d is the chordwise location of y_{max}:

Front percentage = $\frac{y_{front}}{y_{max}}$; where y_{front} is the distance of the sail o¤ the chord line halfway bewteen the leading edge and x_d:

Back percentage = $\frac{y_{back}}{y_{max}}$; where y_{back} is the distance of the sail o¤ the chord line halfway bewteen x_d and the trailing edge.

Leading edge slope is the slope of the tangent to the sail at the leading edge.

Trailing edge slope is the slope of the tangent to the sail at the trailing edge.Using these parameters the sail shape is de…ned using two fourth order bezier curves. The two curves meet at the maximum draft position (x_d), and at this point the curvature is forced to be continuous.

1.1.2 Design parameters

Four di¤erent camber values were tested: 21%, 23%, 25% and 27%, for each camber setting the draft was set at 40%, 45% and 50%. In total this gave 12 di¤erent section shapes. The design with 23%

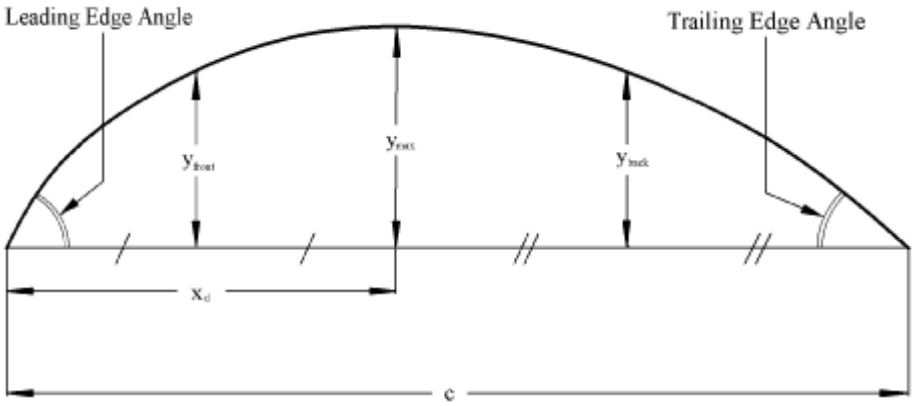

Figure 1.1: A sail section with it's de…ning geometry.

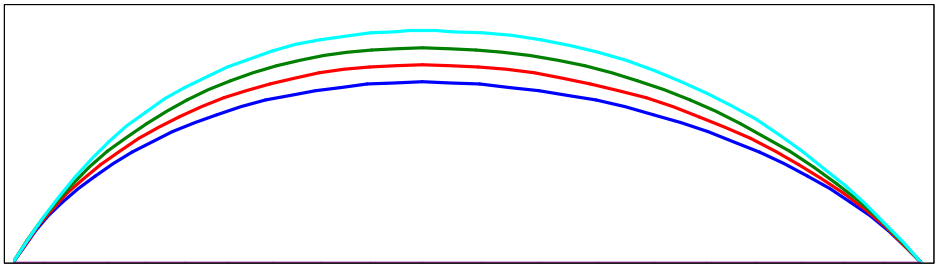

Figure 1.2: Comparison of sails of varying camber (21%, 23%, 25%, 27%) with draft …xed at 45%.

camber and 45% draft was based upon a horizontal slice from a Team New Zealand gennaker ‡ying shape. The range of cambers investigated is illustrated in Figure 1.2, where four sail shapes with 21%, 23%, 25% and 27% camber are plotted, each sail has 45% draft. In …gure 1.3 three sail shapes are plotted with 40%, 45% and 50% draft, each sail has 23% camber. For all sails tested in this study the leading and trailing edge slopes were …xed at 60 and 50 degrees respectively and the front and back precentages were set at 82.45% and 79.87% respectively. For the sails tested in this chapter a naming convention was used in the format XXYY where XX is the camber and YY is the draft, i.e., section 2345 has 23% camber and 45% draft.

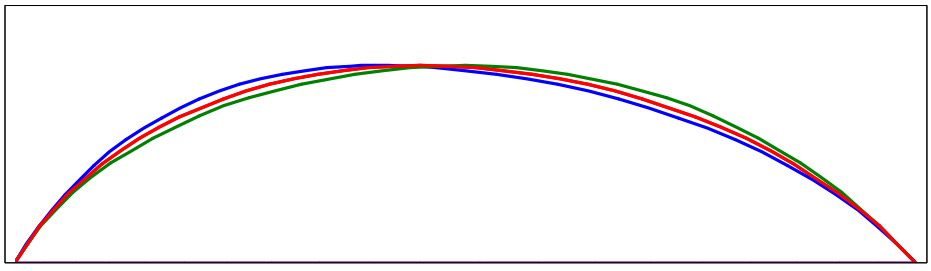

Figure 1.3: Comparison of sails of varying draft (40%, 45%, 50%) with camber …xed at 23%.

1.1.3 Analysis proceedure

On an average downind course IACC yachts sail with an apparent wind angle of approximately 90±*:* Consequently the lift force is the primary contributor to the yachts driving force and the drag force has more in‡uence on the yachts heeling moment and side force. Therefore downwind sails are designed and trimmed in order to maximise lift while paying little consideration to drag. Even when sailing at deep angles where the drag contributes to driving force (i.e above 90±), the increase in drag that is experienced at angles above the maximum lift angle (i.e post stall) does not succesfully compensate for the loss of lift due to stall. Consequently downwind sails are always trimmed to maximum lift.

As a yacht sails downwind the wind strength and direction is continually changing - at times dramatically - and consequently both the yacht's direction and the sail trim must be continually adjusted. However through all these changes the sails are still trimmed to achieve maximum lift and hense provided the section shapes of the sails remain constant (or a sail change does not take place) then the angle of attack of the wind to the chord line of the sail remains constant. Consequently it is possible to evaluate a particular sail shape through all conditions by deteriming it's lift and drag coe¢cient at maximum lift and resolving the drive and side forces across a range of apparent wind angles. This does however neglect and Reynolds number e¤ects that may occur as the apparent wind speed changes.

For the current study the force coe¢cients were measured at four di¤erent angles of attack around the angle of maximum lift. For most sail sections the maximum lift angle was approximately 20± §2± and suitably the forces were evaluated at ® =15±, 17.5±, 20± and 22.5±*:* The forces were then …tted with a cubic polynomial and the lift coe¢cients at maximum lift were determined from this …t. In order to evaluate the accuracy of this method simulations were preformed at several other angles of attack for the base design (camber = 23%, draft = 45%). The results of this investigation are presented in Section 1.2.3.

1.1.4 The CFX model

In this study the sail sections were modelled as a in…nately thin wall in the same fashion as in Chapter ??. The domain dimensions are illustrated in Figure 1.4. At the inlet cartesian velocity components are speci…ed according to the angle of incidence. For all simulations the chord lenth was set a 1*m* and the Reynolds number based on chord length was set at 3308706 which is a typical Reynolds number for IACC spinnakers and gennakers. For a typical downwind sail mid girth (chord length ' 14*m* at mid grith) this Reynolds number corrosponds to apparent wind speed of approximately 3.5*m:s*^{i1} or 7 knots. For IACC yachts 7 knots of apparent wind is obtained in 10 to 15 knots of true wind speed which is an average wind range for the Hauraki Gulf. At the inlet the freestream turbulence intensity was set at 1% with a length scale of 0.001*m*. [mention earlier that solutions are independent of freestream turbulence.] At the outlet a zero static pressure gradient boundary condition was imposed.

The grids were generated in ICEM-HEXA. Three levels of re…nement were used and the grids are referred to as coarse, medium and …ne with 13200, 55380 and 225940 cells respectively. A grid convergence study is presented in Section 1.2.2. At each re…nement level the number of nodes along

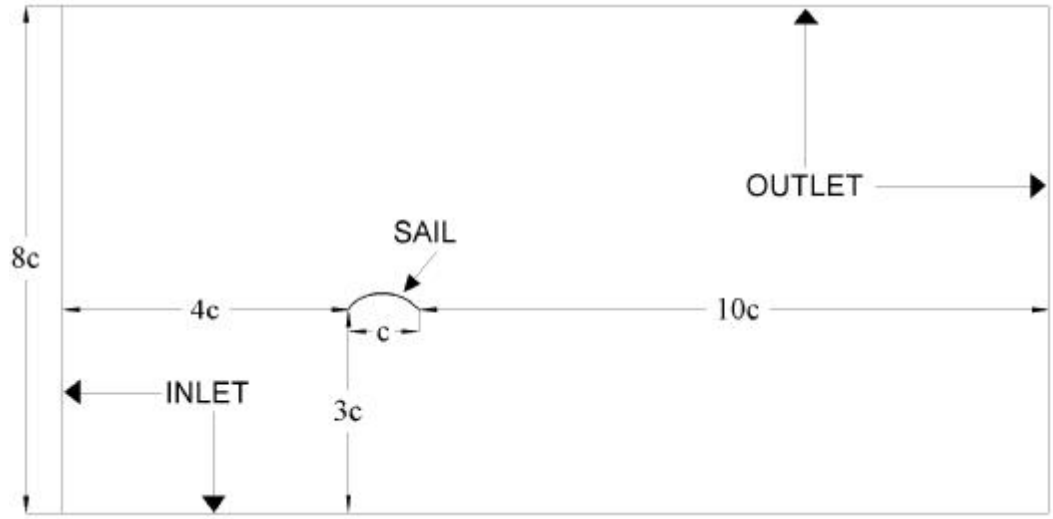

Figure 1.4: Details of the domain for the design study.

every block boundary was doubled. The medium grid is illustrated in Figure 6. In order to achieve a y^+ of approximately 1:0 the near wall spacing was set at 6:25 £ 10 i 5c. Particular care was taken to provide high quality cells around the leading and trailing edges and in these regions the cells have an aspect ratio of 1 : 1, the leading edge region is illustrated in the close-up view in Figure 1.5. Further down the chord very high aspect ratio cells are used in order to resolve the large ‡ow gradients normal to the wall.

For all simulations the SST turbulence model was used. Time integration was performed using second-order backward euler time stepping and interpolation of the advection term was achieved using the high resolution upwind scheme.

1.2 Results

1.2.1 Time step convergence study

Time step convergence was investigated by starting with a time step of 0.00125s and then repeating the simulations with the time step halved and then halved again, i.e. the time step sizes used are 0.00125s; 0.000625s and 0.0003125s: While simulations were performed at each angle of attack (® = 15±; 17:5±; 20± and 22:5±), only the results for ® = 15 are presented since the period of vortex shedding increases as the angle of attack is increased. In Figure 1.6 the lift and drag coe¢cients are presented for the sequence of time step sizes.

As the timestep size is reduced both the lift and drag coe¢cients level indicating satisfactory time step convergence. The lift for the solution using the medium time step is within 0.075% of the lift computed using the short time step and the drag is within 0.19%. The medium time step size corresponds to approximately 33 time steps per shedding cycle.

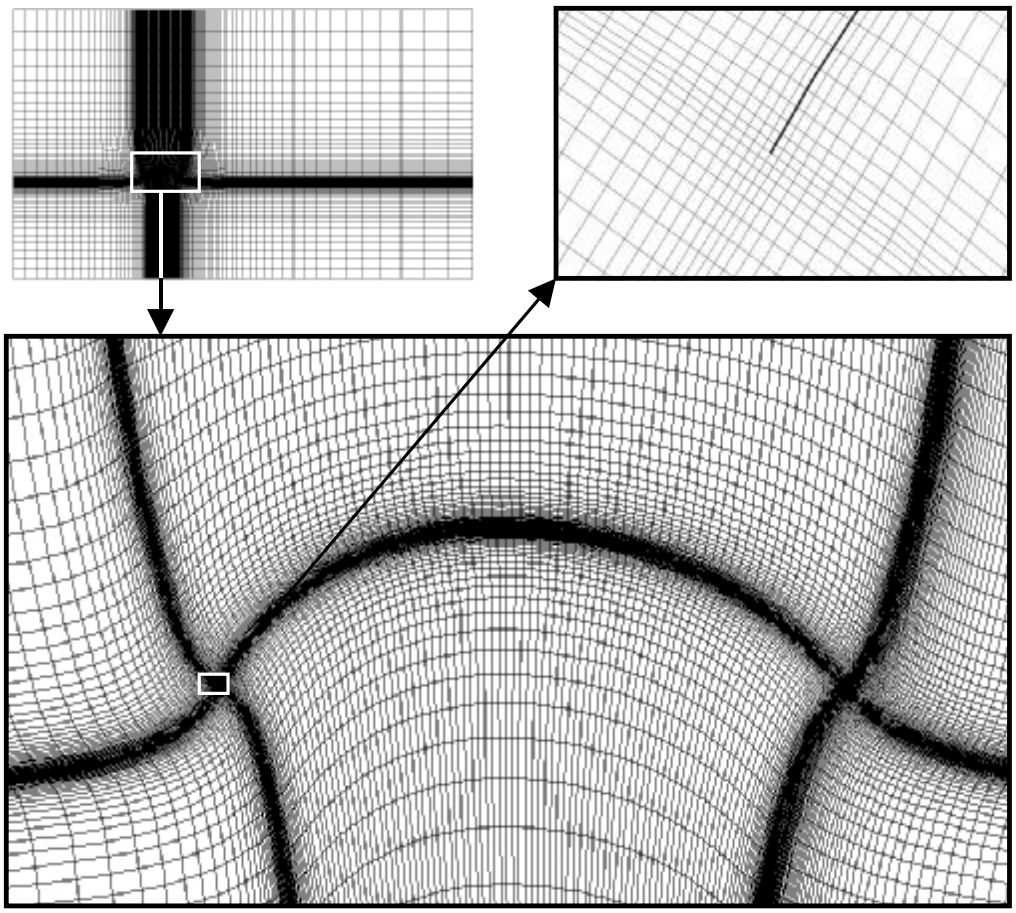

Figure 1.5: Computational grid for the design study (section 2345) (medium grid).

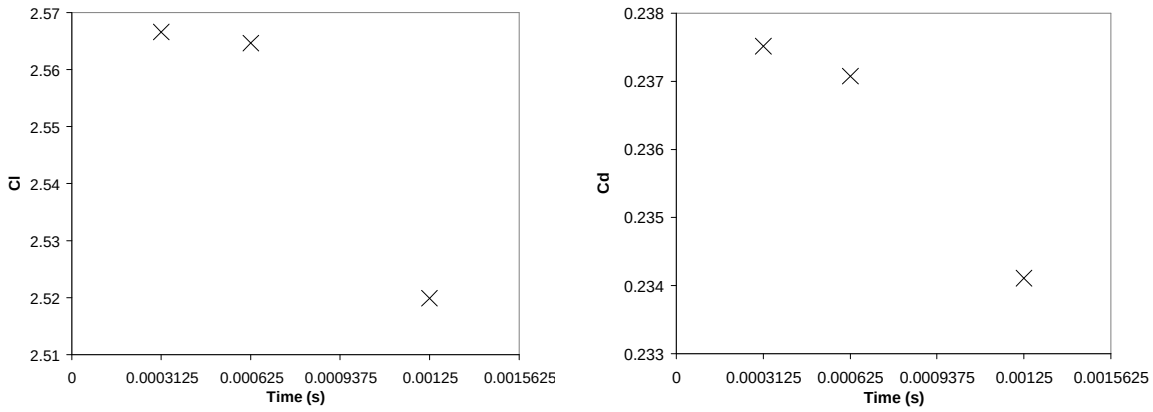

Figure 1.6: Time step convergence of the lift and drag coe¢cients (® = 15).

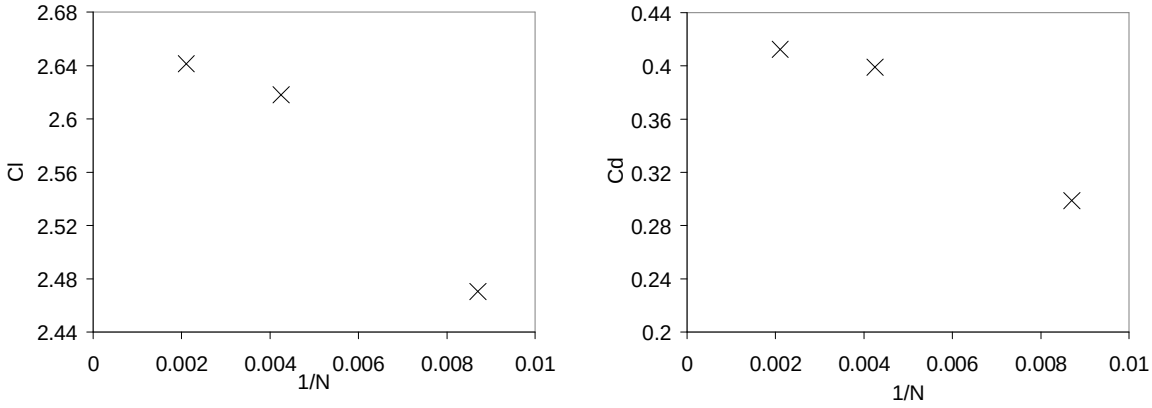

Figure 1.7: Grid convergence of the lift and drag coe¢cients.

1.2.2 Grid convergence study

The grid convergence study was performed at ® = 20± which is approximately the angle where maximum lift occurs. Lift and drag coe¢cients are presented in Figure 1.7 for the sequence of grids. The force coe¢cients are plotted against 1=*N* [*m*] which is a measure of the grid spacing where N^2 is the total number of cells in the grid.

As the grid is re…ned there is a clear convergence of the lift and drag coe¢cients as the grid is re…ned. The lift from the medium grid solution is within 0.9% of the …ne grid solution and the drag is within 3.33%. The accuracy of the medium grid solution is not entirely pleasing with the drag in particular showing considerable grid dependence. However the drag has little in‡uence on the performance of a sail section and many simulations were required in this study and hense using the …ne grid would have been too time consuming. Hense it was decided that the medium grid was the most suitable gird, and that it would at least provide su¢cient accuracy for qualitative analysis of the design space.

1.2.3 Behaviour of the base section shape

The lift versus angle of attack characteristics for the 2345 section is presented in Figure ??. Also plotted in red is a polynomial …t through the data points at 15±; 17.5±; 20± and 22.5± (highlighted in blue). The …tted curve estimates the maximum lift coe¢cient to be 2.62 and to occur at 20.22± and the …tted curve agrees well with the data points at 18.75± and 21.25±: The lift curve in Figure ?? has the same general shape as the was found in the validation study (Chapter ??).

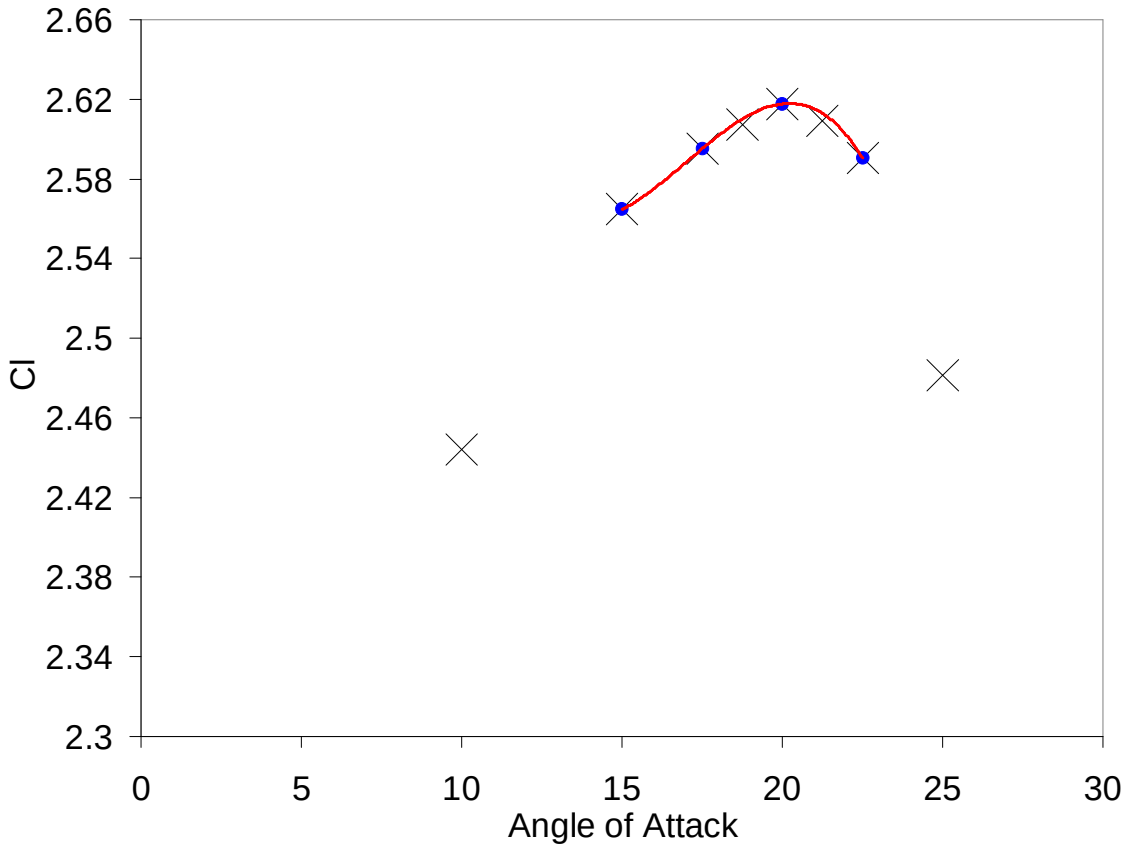

Figure 1.8: